SUPPLEMENTAL INFORMATION

Supplemental Figure Legends

Figure S1. Correlative LM/ESI-tomography and chemical fixation and plastic embedding does not perturb 30 nm or higher-order chromatin fibre assemblies. **A** An overlaid image of the fluorescence signal generated from an H3K9me3 antibody on section with the phosphorus enhanced mass image of a mouse embryonic fibroblast (MEF) nucleus. Black boxes indicate regions where high magnification tomography data sets were acquired. **B** A central slice from a tomogram of a non-H3K9me3 labelled 'open' region within the MEF and **C** within the 'closed' heterochromatin domain. Both contain 10nm fibres. **D** Image of a MEF chromocentre from a sample preserved by cryo-fixation reveals chromatin fibre structures, which are morphologically identical to those seen in samples prepared by chemical (paraformaldehyde/glutaraldehyde) fixation. Shown in **E** is a tomogram of central slice of MEF chromocentre where all chromatin fibres can now be resolved, revealing 10 nm fibres within the compact heterochromatin chromocentre and also in the surrounding open chromatin domains in the cryo-fixed samples. Scale bar represents 0.75 μm in panels B and C and 0.5 μm in panels D and E.

Figure S2. Bending and folding of 10 nm chromatin fibres are sufficient to form the compact and open chromatin fibre domains in mouse embryonic fibroblasts and in mouse tissues. Model of an averaged tomogram through a central slice processed to reduce signal noise with Chimera and pseudo coloured yellow emphasizing continuous 10 nm

chromatin fibres and enabling visualization of fibre bending in the two dimensional representation of a mouse embryonic fibroblast chromocentre **A**; a lymphocyte from spleen tissue **C**; and a tissue liver cell **E**. Digitally zoomed image of the region indicated by the white box of each cell type or tissue type respectively **B**, **D** and **F**, where fibre-fibre packaging and spacing are now clearly visible. Scale bar represents 500 nm in panels **A**, **C** and **E**; and 30 nm in **B**, **D** and **F**.

Figure S3. Image and Fourier Transform analyses are consistent with an exclusively 10 nm chromatin organization in mouse nuclei. **A** Tomographic reconstruction of a spleen lymphocyte with black boxes showing regions digitally enhanced and highlighted in panels **B** and **D.** **B** illustrates a number of ribosomes associated with the ER. The red arrows indicate a ribosome represented within the field. After processing these samples for EM and tomographic reconstruction the dimensions of these ribosomes are approximately 21 nm in diameter. **C** Canny edge detection from the densely packed chromatin domain shown in **D** was used to make Fourier measurements of both chromatin fibre dimensions and regular chromatin fibre spacings. Yellow arrows indicate an example of a 10 nm chromatin fibre in both the edge detection image **C** and the averaged phosphorus tomographic volume shown in **D**. Yellow arrowheads indicate a regular fibre spacing in both panels. Scale bar represents 0.5 μm in panel **A** and 30 nm in panels **B-D.** **E** shows the Fourier spectra of the edge-detected image (C) with the resolution of the peaks in the table.

Supplemental Movie Legends

Supplemental Movie 1. 10 nm chromatin fibres of both the closed compact domain of a mouse embryonic fibroblast (MEF) chromocentre and the surrounding open dispersed chromatin are visible in the phosphorus map tomogram. The sequential slices of the 3D phosphorus tomogram enable measurements of the 10 nm chromatin fibres, which populate both domains. Chromatin fibres are frequently observed crossing over one another within the 70 nm section. Scale bar is 100 nm.

Supplemental Movie 2. Canonical "beads-on-a-string" 10 nm chromatin fibres are readily distinguished by high-resolution tomographic reconstructions of Phosphorus-maps. This movie shows a string of nucleosomes and intervening linker DNA, rotated to reveal these features. Surrounding chromatin fibres were masked for clarity. Scale bar represents 30 nm.

Supplemental Movie 3. DNA wrapping around the core histone proteins can be visualized in tomographic reconstructions of phosphorus maps. Since these are phosphorus maps the *en face* views of nucleosomes result in a clearly defined hole in the phosphorus signal. This movie shows a nucleosome that is rotated in 3D to reveal both the *en face* view and the side view of this representative nucleosome. The surrounding chromatin was masked for clarity. Scale bar represents 30 nm.

Supplemental Materials and Methods

Limitations of conventional transmission electron microscopy approaches

ESI analysis of nuclear structures is particularly powerful as it provides both biochemical and structural information of *in situ* samples without the use of contrast enhancing reagents, which can obscure valuable fine structural detail. For instance, using ESI analysis we have previously been able to identify some 10 nm chromatin fibre structures even in regions of densely packaged chromatin fibres in MEF chromocentres (Fussner et al., 2011). However, previous studies using contrast-enhancing reagents were unable to detect these fibre structures and resulted in measurements of chromocentre domains as exclusively higher-order chromatin fibre assemblies (Rego et al., 2008). In densely packed chromatin domains, resolving the absolute chromatin fibre configuration is often difficult or impossible, even when using ESI. This is due to the fact that the images are projections, where all the chromatin fibres in the z-direction are projected onto a 2-dimensional plane. Although ESI has an exceptional capacity to resolve individual nucleosomes and intervening linker sequences *in situ* it also suffers from the projection of 3-dimensions onto a 2-dimensional image plane. We have previously demonstrated that ESI is capable of detecting all the chromatin and nucleosomes in *in situ* nuclei (Fussner et al., 2010; Fussner et al., 2011). Consequently combining ESI with electron tomography has enabled us to overcome the projection limitation and provides high-contrast, high-resolution net phosphorus images that reveal chromatin fibres *in situ* in 3-dimensions. Thus, we are now able to resolve the structure of each individual chromatin fibre in both open and closed compact domains.

Advantages and Caveats of ESI-tomography

Combining electron tomography with ESI enabled us to generate three-dimensional images of chromatin fibres *in situ* with sufficient resolution to describe the higher-order fibre folding and fibre conformation in mouse tissue and cells. In addition to describing the chromatin structure with significant detail, ESI-tomography of phosphorus maps also generates exceptionally high-contrast images of RNA-based molecules. RNA-protein complexes are well contrasted in the space between compact chromatin domains (e.g. in spleen lymphocytes (Figure 4)).

Tissue preparation and cell culture

Patiria miniata testis were isolated by dissection and fixed overnight in 2% glutaraldehyde (GA). Mouse tissues were also isolated by dissection and then sieved to separate cells prior to overnight fixation in 2% GA.

Primary mouse embryonic fibroblasts (MEFs) were isolated from day 15.5 mouse embryos and cultured in standard DMEM and 10% FBS. Cells were fixed with 2% paraformaldehyde, 0.5% triton permeabilized, antibody labelled for H3K9me3 histones with a rabbit antibody (generous gift from Dr. Prim Singh) and visualized with a Cy3 (Jackson labs) secondary antibody and post-fixed with 1% glutaraldehyde and dehydrated with an ethanol series. In fixation control experiments, immortalized MEFs were slam frozen in liquid nitrogen and infiltrated with resin by freeze-substitution. ESI is capable of detecting the phosphorus signal contributed by the phospholipid bilayer *in situ* only when an osmium post-fixation step is used, where osmium tetroxide crosslinks the

bilayer's protein and lipid components. Because this fixation step was not required in our study, the phospholipids were extracted during dehydration, and therefore were not visualized.

All samples were embedded in either Quetol or LRwhite as previously described (Ahmed et al., 2009) and sectioned with a Leica ultramicrotome into 70 nm sections and then coated with a 3 nm film of carbon to improve sample stability. 10 nm gold particles were used on section as fiducial markers for tomographic reconstructions.

Correlative LM/ESI

Heterochromatin domains in MEF cells were identified after sample preparation denoted above using a Leica epifluorescence microscope with a 63X objective lens. Fluorescence from the heterochromatin domains is readily detected in these cells in the 70 nm section (Fussner et al., 2011). Fluorescence images are correlated to low magnification phosphorus-enriched mass images acquired on an FEI Tecnai20 transmission electron microscope equipped with a GATAN Imaging Filter, at 155eV and 120eV energy loss as previously described (Ahmed et al., 2009).

ESI-Tomography

SerialEM (Mastronarde, 2005) software, was used to acquire the high-magnification phosphorus tilt series. The tilt range was +/- 60° with phosphorus ESI image pairs collected at 120eV and 155eV every 2°. Image stacks were aligned using IMOD (Kremer et al., 1996), and processed into phosphorus ratio maps using IMOD, SPARX (Hohn et al., 2007) and ImageJ. The SIRT algorithm (IMOD implementation)

was used to generate 3D phosphorus maps from the aligned image series. Chimera was used to render 3D images and generate perspective maps and movies.

Combined zero tilt phosphorus and nitrogen images using ESI were acquired at 120eV and 155eV, and 385eV and 415eV to generate the phosphorus and nitrogen ratio maps, respectively. Nitrogen maps were normalized to zero in chromatin-rich regions and the phosphorus maps were overlaid onto the nitrogen normalized images to represent chromatin, pseudo coloured in yellow and protein-rich structures, pseudo coloured in blue.

Data Analysis

ESI images were processed using Adobe Photoshop 7.0 as previously described (Ahmed et al., 2009). Line scans to measure fibre densities and fibre spacing were performed using Digital Micrograph.

The Fourier transform of an image is highly sensitive to the distance information present in an image. By summing the rotationally averaged power spectra (modulus squared of the Fourier transform) of overlapping windows of areas of interest, we can obtain the relative frequency of distance repeats expressed in reciprocal distance units. However, since we are interested in measuring not only fibre spacing but also fibre width, we developed a method of measuring both the width of the fibre and the spacing between fibres through the use of edge detection.

Each image was median filtered to reduce high frequency speckle noise, and then the edges of the fibres found using Canny edge detection, as implemented in FeatureJ, a plugin of ImageJ. The Fourier analysis described in the Materials and Methods section,

performed on the edge detection images now provide spectra that show average fibre widths and spacings between fibre edges. The peaks can then be interpreted by comparing the original image of the fibres with the peaks to determine which are spacings between fibres, spacings plus fibres, or fibre dimensions themselves.

The real advantage of this analysis technique over manual measurements in real space is that it measures many fibres simultaneously, and it enables detection of repeats that are not obvious to the human eye.

Supplementary References

Ahmed, K., Li, R., and Bazett-Jones, D.P. (2009). Electron spectroscopic imaging of the nuclear landscape. Methods Mol Biol *464*, 415-423.

Fussner, E., Ahmed, K., Dehghani, H., Strauss, M., and Bazett-Jones, D.P. (2010). Changes in chromatin fiber density as a marker for pluripotency. Cold Spring Harb Symp Quant Biol *75*, 245-249.

Fussner, E., Djuric, U., Strauss, M., Hotta, A., Perez-Iratxeta, C., Lanner, F., Dilworth, F.J., Ellis, J., and Bazett-Jones, D.P. (2011). Constitutive heterochromatin reorganization during somatic cell reprogramming. EMBO J.

Hohn, M., Tang, G., Goodyear, G., Baldwin, P.R., Huang, Z., Penczek, P.A., Yang, C., Glaeser, R.M., Adams, P.D., and Ludtke, S.J. (2007). SPARX, a new environment for Cryo-EM image processing. J Struct Biol *157*, 47-55.

Kremer, J.R., Mastronarde, D.N., and McIntosh, J.R. (1996). Computer visualization of three-dimensional image data using IMOD. J Struct Biol *116*, 71-76.

Mastronarde, D.N. (2005). Automated electron microscope tomography using robust prediction of specimen movements. J Struct Biol *152*, 36-51.

Rego, A., Sinclair, P.B., Tao, W., Kireev, I., and Belmont, A.S. (2008). The facultative heterochromatin of the inactive X chromosome has a distinctive condensed ultrastructure. J Cell Sci *121*, 1119-1127.

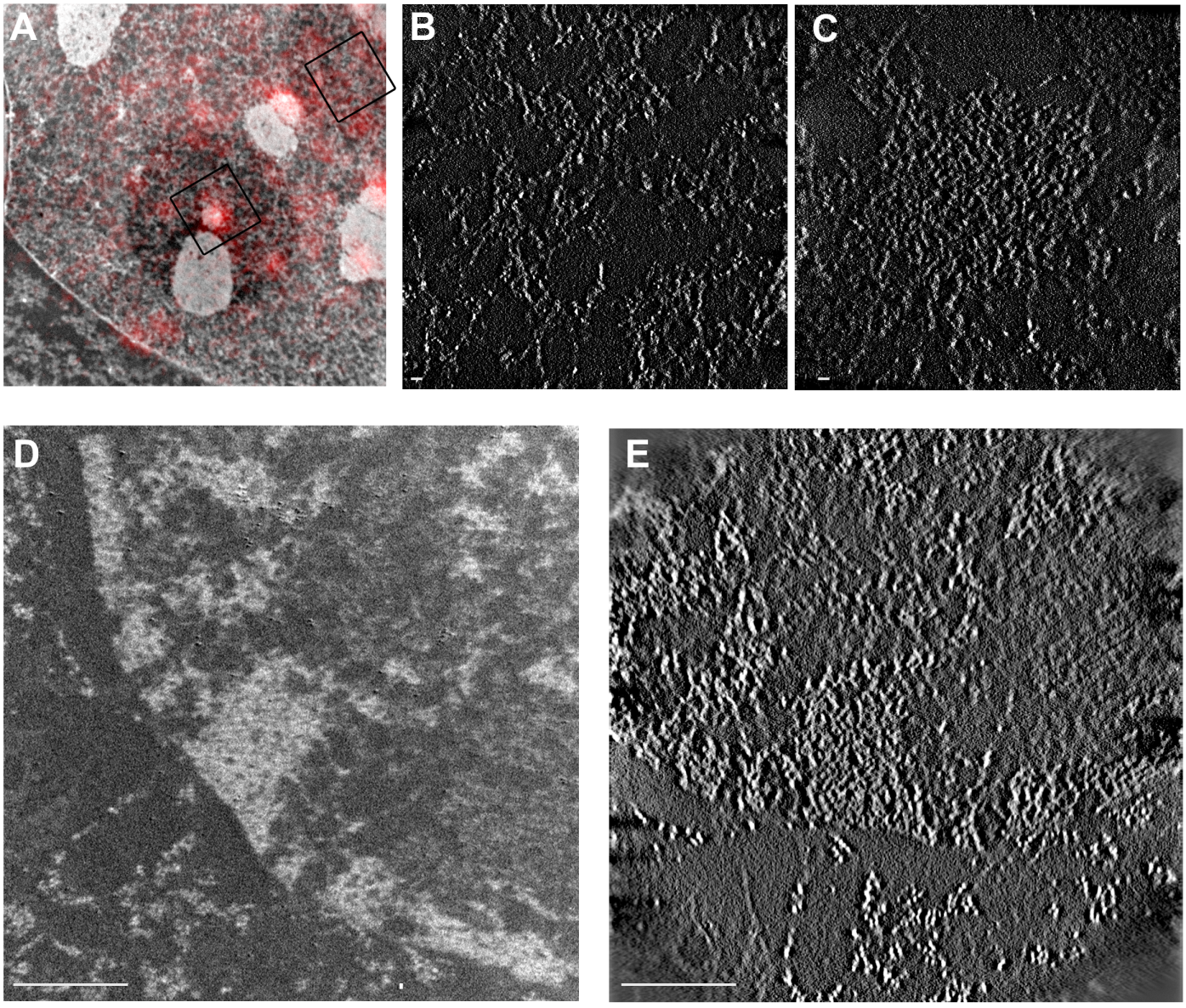
A
B
C
D
E

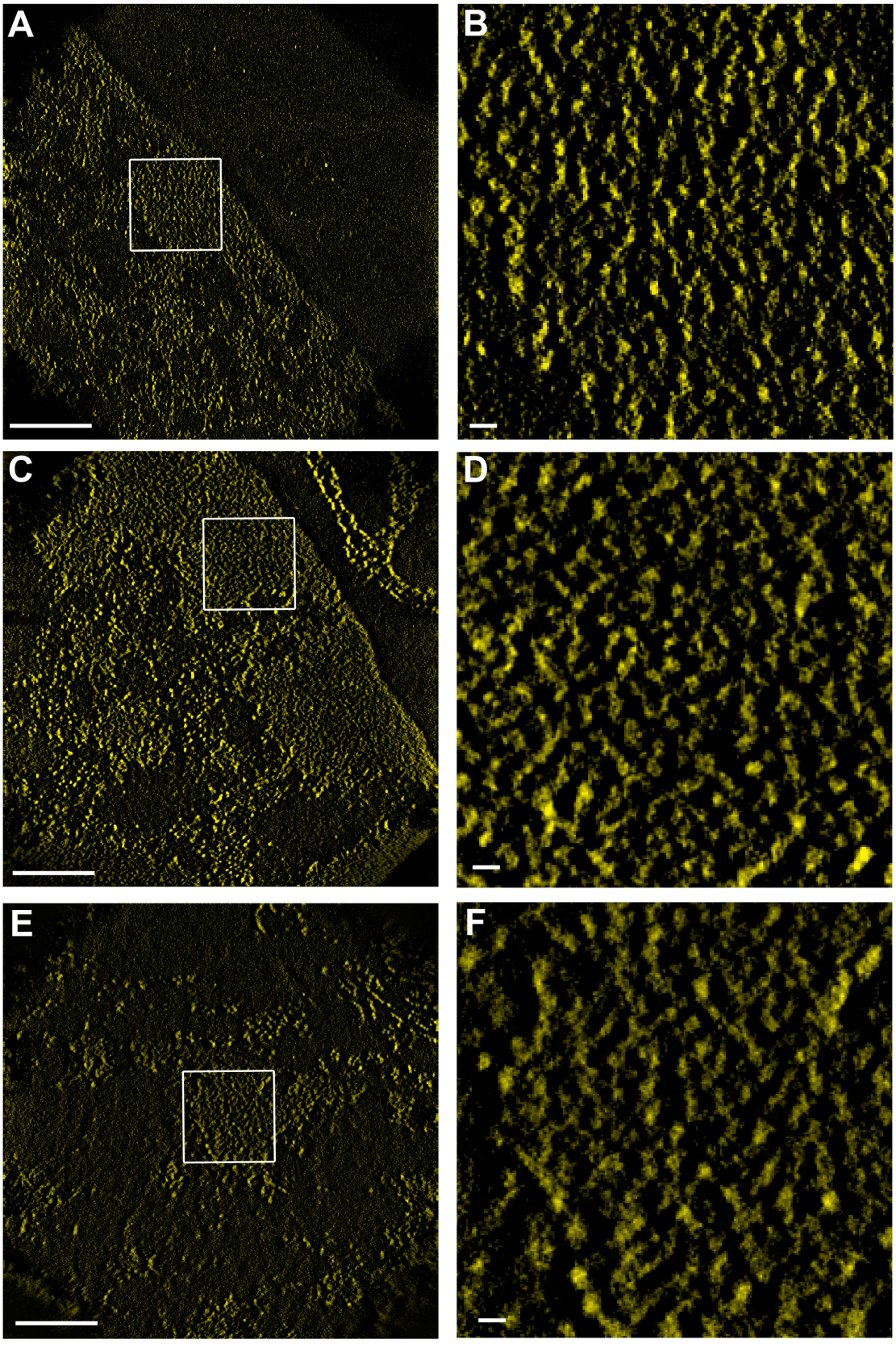
A
B
C
D
E
F

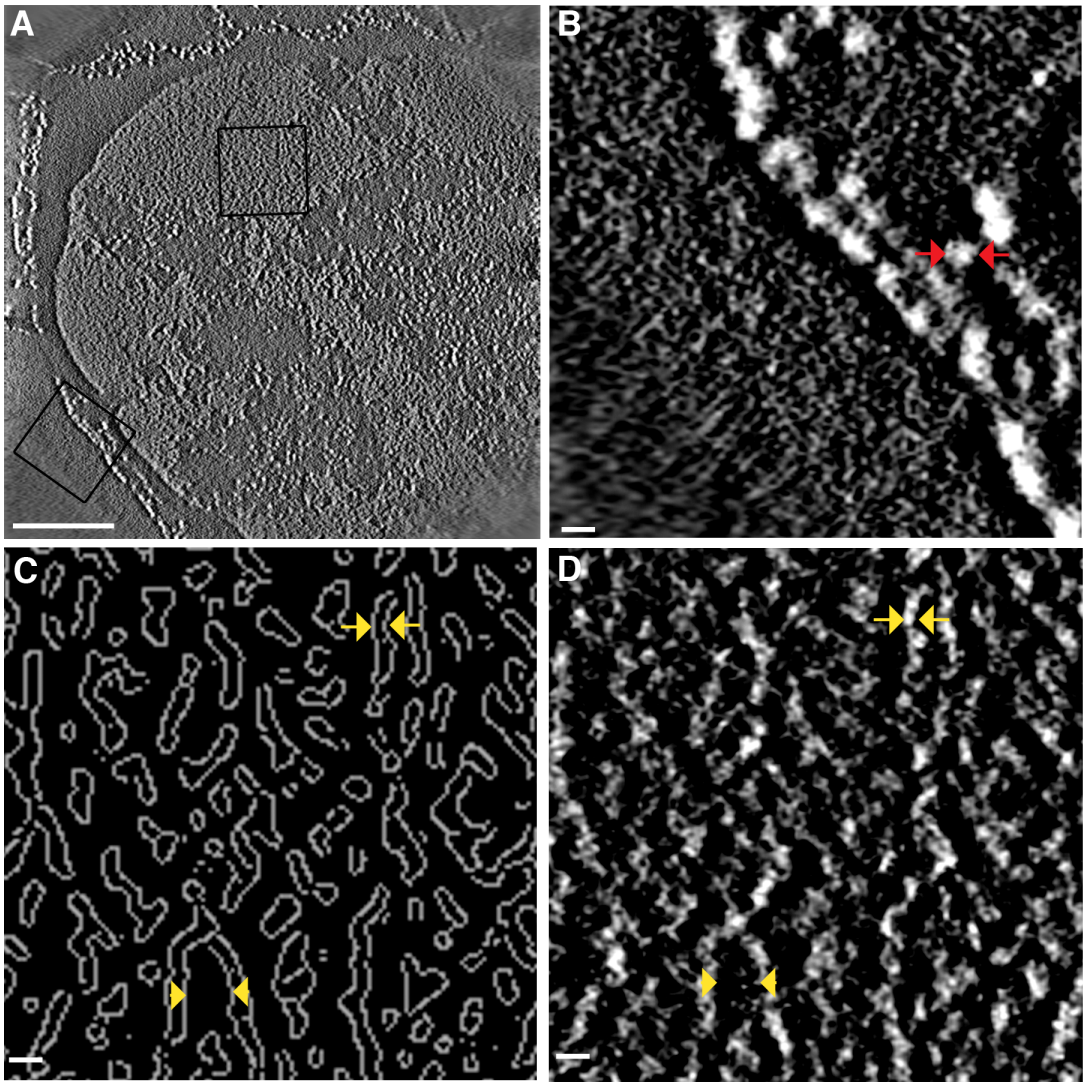

E

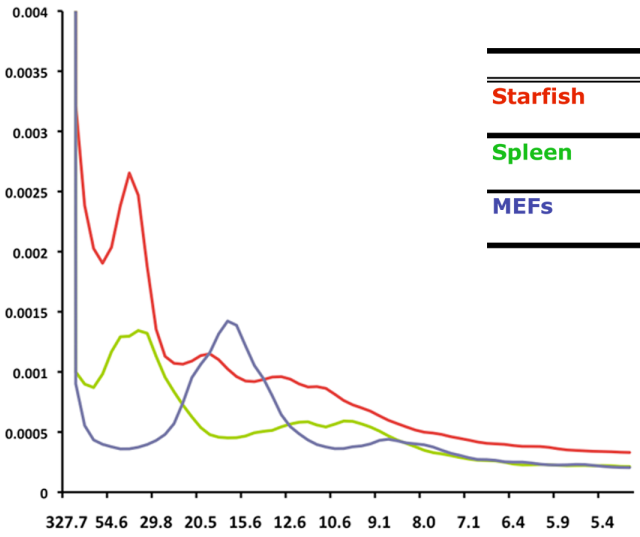

	Frequency (1/nm)	Size or Spacing (nm)
Starfish	0.023	43
	0.05	20
Spleen	0.025	39
	0.098	10
MEFs	0.054	19
	0.11	9